JOC Article
pubs.acs.org/joc

Design, Validation, and Implementation of a Rapid-Injection NMR System

Scott E. Denmark,* Bruce J. Williams,*,† Brian M. Eklov, Son M. Pham, and Gregory L. Beutner

Roger Adams Laboratory, Department of Chemistry, University of Illinois, Urbana, Illinois 61801

sdenmark@illinois.edu

Received April 29, 2010

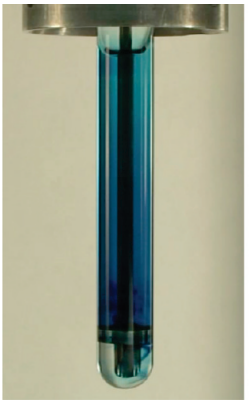

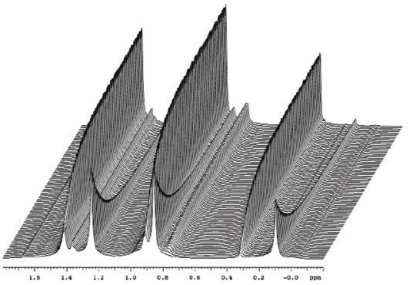

A Rapid Injection NMR (RINMR) apparatus has been designed and constructed to allow the observation of fast chemical reactions in real time by NMR spectroscopy. The instrument was designed to allow the rapid (< 2 s) injection and mixing of a metered volume of a reagent into a spinning NMR tube followed by rapid acquisition of the data resulting from the evolution of the chemical process. The various design criteria for this universal system included the ability to deliver any chemical reagent at any temperature and allow for the observation of any nucleus. The various challenges associated with the construction and implementation of this instrument are documented along with the validation of the accuracy of the apparatus with respect to volume and temperature. Finally, the ultimate validation and reproducibility of the technique is presented in the form of three case studies that used the instrument to elucidate various aspects of organic reaction mechanisms. The authors urge interested parties to not embark on the construction of their own instrument and invite those whose research problems might be amenable to this kind of analysis to contact the corresponding author for access to the apparatus described herein.

Introduction

The foundation of modern synthetic organic chemistry rests firmly on the bedrock that is physical organic chemistry. Without the unifying principles that correlate structure with reactivity and selectivity, the universe of synthetic transformations would seem a bewildering collection of empirical experience. It is therefore axiomatic that each new advance in synthetic methodology should be evaluated in the context of current mechanistic paradigms. If the new process can be understood and rendered predictable within the framework of modern theory, then the theory has survived a critical test. If the new process cannot be understood, then the origin of the deviation should be identified and current theory modified to accommodate the new data. In either scenario, a thorough understanding of the factors that influence the new chemical transformation (rate, stereoselectivity, substrate scope, byproducts) is needed. Regrettably, this is rarely the case despite the spectacular advances over the past decades in spectroscopic, analytical, and computational methods.

†Correspondence author for all inquires relating to design and construction of the instrument. Email: williams@scs.illinois.edu.

Published on Web 07/30/2010 DOI: 10.1021/jo100837a

In the late 1990s a new family of catalytic, asymmetric transformations was developed in these laboratories that involved the use of chiral Lewis bases in conjunction with Lewis acidic silicon compounds to effect carbonyl addition (allylation, aldolization) and epoxide opening reactions.[1] Because the basis of this new type of catalysis was poorly understood, a comprehensive program designed to elucidate the critical features of (1) reaction scope and stereoselectivity,[2] (2) Lewis base−Lewis acid structure in the solid state and in solution,[3] and (3) structure of reactive intermediates and reaction kinetics (turnover-limiting and stereochemistry-determining steps) was launched.[4] The first two objectives could be met by the use of well-established protocols, but the third represented greater challenges in view of the extraordinary rapid rates of reaction. Of course, many experimental techniques have been developed to determine the kinetic behavior of reactions in solution and to identify reactive intermediates including stop-flow UV−vis spectroscopy[5] and *in situ* IR spectroscopy.[6] Although each of these techniques has their individual advantages and limitations, they can provide a wealth of information when applied appropriately. Indeed, early in these studies, the use of *in situ* IR spectroscopy allowed real-time monitoring of slower reactions (section 7.1). This instrument performs quite well for substrates with strong infrared absorbances and where reaction concentrations can be adjusted to obtain an appropriate signal-to-noise ratio without extending analysis times. However, for faster reactions executed at high dilution, *in situ* IR analysis was ineffective in obtaining meaningful kinetic data. Moreover, this technique pales in comparison to high field NMR spectroscopy for the structural determination of reactive intermediates and determination of kinetic profiles in temperature ranges from −150 to + 150 °C. In addition, the availability of highly sensitive probes made NMR spectroscopy an ideal analytical tool for interrogating chemical transformations at high dilution in real time.

Yet despite the exquisite sensitivity, ability to operate over a wide range of temperatures, and wealth of structural information, NMR spectroscopy is experimentally a much more complicated technique. The manifold difficulties are immediately apparent and include rapidly delivering a known amount of a temperature-equilibrated reagent into a temperature-equilibrated substrate while the sample is spinning in the NMR spectrometer and ready for acquisition, all while coordinating the injection event with data acquisition. In addition, care must then be taken to ensure that the data is collected in a manner that produces integral values that are not only internally consistent (resonance to resonance within a single spectrum) but also consistent between the plethora of spectra collected over the course of an individual experiment. An instrument that addresses these challenges was introduced already 30 years ago by McGarrity,[7] and since then the technique has been implemented in a number of laboratories. Our objectives were to take the basic concept and redesign the instrument for use in high sensitivity, modern NMR spectrometers and to address 21st century problems in organic reaction mechanisms.

Background

Since the initial reports by McGarrity and co-workers,[7] Rapid Injection NMR (RINMR) has become an invaluable tool for the study of reaction mechanisms. The original McGarrity apparatus consists of an injection assembly containing a gastight syringe coupled to a long injection capillary terminated with a perforated bulb. Once completely lowered into the magnet, the bulb rests just below the reaction sample in the NMR tube. The syringe is driven by a pneumatic piston whose course is set by a micrometer screw. Movement of the piston triggers the spectrometer pulse and acquisition sequence. A major drawback of this design is that the syringe and capillary remain stationary throughout the experiment allowing diffusion of the injection liquid from the capillary bulb into the reaction medium inside the spinning NMR tube. Additionally, the injection assembly and capillary causes a perturbation of the magnetic field homogeneity resulting in peak broadening. Although this effect is minimal under slow acquisition conditions, peak broadening is unavoidable for fast reactions. Even with these limitations, various groups have successfully utilized the McGarrity technique to observe reactive intermediates as well as to determine reaction kinetics.[8] Further demonstrating its utility, Klein and Gawley reported using the RINMR technique originally developed for proton observation to study the kinetics of tin−lithium transmetalation using ^{119}Sn NMR analysis.[9]

(1) (a) Denmark, S. E.; Beutner, G. L. *Angew. Chem., Int. Ed.* **2008**, *47*, 1560–1638. (b) Denmark, S. E.; Fujimori, S. In *Modern Aldol Reactions*; Mahrwald, R., Ed.; Wiley-VCH: Weinheim, 2004, Vol. 2, Chapter 7. (c) Denmark, S. E.; Stavenger, R. A. *Acc. Chem. Res.* **2000**, *33*, 432–440. (d) Denmark, S. E.; Barsanti, P. A.; Beutner, G. L.; Wilson, T. W. *Adv. Synth. Catal.* **2007**, *349*, 567–582.

(2) (a) Denmark., S. E.; Chung, W.-j. *J. Org. Chem.* **2008**, *73*, 4582–4595. (b) Denmark, S. E.; Ghosh, S. K. *Tetrahedron* **2007**, *63*, 8636–8644. (c) Denmark, S. E.; Fan, Y.; Eastgate, M. D. *J. Org. Chem.* **2005**, *70*, 5235–5248. (d) Denmark, S. E.; Beutner, G. L.; Wynn, T.; Eastgate, M. D. *J. Am. Chem. Soc.* **2005**, *127*, 3774–3789. (e) Denmark, S. E.; Fujimori, S.; Pham, S. M. *J. Org. Chem.* **2005**, *70*, 10823–10840.

(3) (a) Denmark, S. E.; Eklov, B. M. *Chem.—Eur. J.* **2008**, *14*, 234–239. (b) Denmark, S. E.; Fu, J. *J. Am. Chem. Soc.* **2003**, *125*, 2208–2216. (c) Denmark, S. E.; Su, X. *Tetrahedron* **1999**, *55*, 8727–8738.

(4) (a) Denmark, S. E.; Eklov, B. M.; Yao, P. J.; Eastgate, M. D. *J. Am. Chem. Soc.* **2009**, *131*, 11770–11787. (b) Denmark, S. E.; Pham, S. M; Stavenger, R. A.; Su, X.; Wong, K.-T.; Nishigaichi, Y. *J. Org. Chem.* **2006**, *71*, 3904–3922. (b) Denmark, S. E.; Bui, T. *J. Org. Chem.* **2005**, *70*, 10393–10399. (c) Denmark, S. E.; Pham, S. M. *Helv. Chim. Acta* **2000**, *83*, 1846–1853.

(5) Wang, R.-Y. In *Applications of Physical Methods to Inorganic and Bioinorganic Chemistry*; Scott, R. A., Lukehart, C. M., Eds.; John Wiley & Sons: Chichester, 2007; pp 469−487 .

(6) Rein, A. J.; Donahue, S. M.; Pavlosky, M. A. *Curr. Opin. Drug Discovery Dev.* **2000**, *3*, 734–742.

(7) (a) McGarrity, J. F.; Prodolliet, J.; Smyth, T. *Org. Magn. Reson.* **1981**, *17*, 59–65. (b) McGarrity, J. F.; Ogle, C. A. *J. Am. Chem. Soc.* **1985**, *107*, 1805–1810. (c) McGarrity, J. F.; Prodolliet, J. *J. Org. Chem.* **1984**, *49*, 4465–4470. (d) McGarrity, J. F.; Ogle, C. A.; Brich, Z.; Loosli, H. R. *J. Am. Chem. Soc.* **1985**, *107*, 1810–1815.

(8) (a) Frye, S. V.; Eliel, E. L.; Cloux, R. *J. Am. Chem. Soc.* **1987**, *109*, 1862–1863. (b) Chen, X.; Hortelano, E. R.; Eliel, E. L.; Frye, S. V. *J. Am. Chem. Soc.* **1992**, *114*, 1778–1784. (c) Palmer, C. A.; Ogle, C. A.; Arnett, E. M. *J. Am. Chem. Soc.* **1992**, *114*, 5619–5625. (d) Reetz, M. T.; Raguse, B.; Marth, C. F.; Hügel, H. M.; Bach, T.; Fox, D. N. A. *Tetrahedron* **1992**, *48*, 5731–5742. (e) Geletneky, C.; Försterling, F.-H.; Bock, W.; Berger, S. *Chem. Ber.* **1993**, *126*, 2397–2401. (f) Ogle, C. A.; Johnson, H. C., IV; Wang, X. L.; Strickler, F. H.; Bucca, D.; Gordon, B., III. *Macromolecules* **1995**, *28*, 5184–5191. (g) Bertz, S. H.; Carlin, C. M.; Deadwyler, D. A.; Murphy, M. D.; Ogle, C. A.; Seagle, P. H. *J. Am. Chem. Soc.* **2002**, *124*, 13650–13651. (h) Mayr, H.; Ofial, A. R.; Sauer, J.; Schmied, B. *Eur. J. Org. Chem.* **2000**, 2013–2020. (i) Bertz, S. H.; Cope, S.; Murphy, M.; Ogle, C. A.; Taylor, B. J. *J. Am. Chem. Soc.* **2007**, *129*, 7208–7209.

(9) Klein, R.; Gawley, R. E. *J. Am. Chem. Soc.* **2007**, *129*, 4126–4127.

Within the past few years, more sophisticated RINMR instruments have been developed to obviate the limitations of the original design as well as to incorporate features needed for a specific application. One instrument, developed by Mok and co-workers, includes the option for the insertion of an optical fiber for use in photo-CIDNP experiments.[10] Aside from the optical fiber, this device consists of two major parts, a coaxial glass insert fitted inside the NMR tube and a pneumatic injector positioned outside of the magnet. Unique from other devices, the insert is made from a piece of glass capillary tubing fused on one end with a micropipet. The micropipet is positioned just below the surface of the solution in the NMR tube. During injection, the solution held within the capillary is jetted through the micropipet to improve mixing. The use of 5-mm Shigemi tubes further enhances mixing efficiency and greatly reduces the required reaction volume. Because the entire insert is made from glass, it is reasonable to assume that its presence causes minimal disturbance to the field homogeneity.

More recently, an advanced device was reported by Reich and co-workers.[11] In this design, the solvent delivery is similar in practice to the McGarrity device, a syringe housed above the magnet coupled to a long flexible Teflon needle inserted into the NMR tube, but this instrument is designed to house two syringes allowing for multiple injections during a single experiment. Perhaps the most unique aspect of this device is the presence of a mechanical stirrer. The motor is mounted above the magnet, between the syringe housings, and provides efficient mixing down to the solvent freezing point. The raising and lowering of the stirrer paddle as well as injections from either or both syringes can be controlled manually or by the spectrometer pulse program. The authors comment that the instrument was designed to operate with 10-mm NMR tubes to enhance sample sensitivity in multinuclear experiments. While the increased sample size may be advantageous in some situations, it is an unfortunate drawback when more precious reagents are required or when minimal sample volumes are ideal.

Results

1. Design Criteria. Although the basic concept and design of an RINMR apparatus has already been implemented, we envisioned the development of a tool that would far surpass the existing technology in a number of ways. First, to be a truly universal tool, the apparatus must be able to deliver a known amount of any reagent at any temperature under an inert atmosphere and allow for the observation of any nucleus within seconds of injection. Such demands required accurate metering, rapid mixing, and high chemical resistance. Moreover, to be compatible with high field instruments (500−600 MHz ^{1}H) and deliver the high resolution available from such machines, an injection/mixing mechanism was needed that removed the injector from the sample. At the outset of our studies (ca. 1997), no such apparatus was commercially available or described in the literature.

(10) Mok, K. H.; Nagashima, T.; Day, I. J.; Jones, J. A.; Jones, C. J. V.; Dobson, C. M.; Hore, P. J. *J. Am. Chem. Soc.* **2003**, *125*, 12484–12492.

(11) (a) Jones, A. C.; Sanders, A. W.; Bevan, M. J.; Reich, H. J. *J. Am. Chem. Soc.* **2007**, *129*, 3492–3493. (b) Jones, A. C.; Sanders, A. W.; Sikorski, W. H.; Jansen, K. L.; Reich, H. J. *J. Am. Chem. Soc.* **2008**, *130*, 6060–6061.

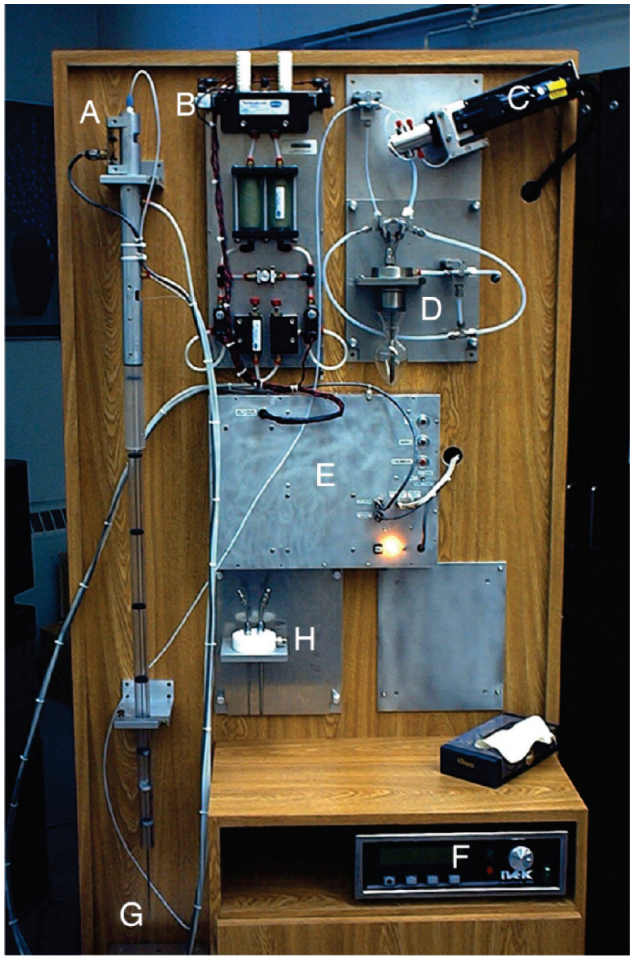

FIGURE 1. Rapid Injection NMR apparatus. (A) Optical sensors for injector travel stops. (B) Pneumatic valve system to actuate injector piston. (C) Ivek metering pump. (D) Reservoir flask and inert atmosphere valves. (E) Electronics module. (F) Metering pump controller. (G) Injector tip. (H) Injector rinse adapter.

2. Construction. The extreme demands on performance set out above and the highly interdisciplinary nature of the project would require the coordinated efforts of many individuals. Fortunately, the design, fabrication, and spectroscopic facilities at the University of Illinois are outstanding. A team was assembled that included an electrical engineer (B.J.W.), spectroscopist (Paul Molitor), machinist (Bill Knight), and designers/users (S.E.D. and S.M.P.). The first step in the process was to secure the RINMR apparatus developed by McGarrity, which was kindly provided by Eliel, who has employed it for many studies.[8] Although inspirational, this apparatus was deemed too crude for the objective outlined above, and accordingly, a totally new design was implemented. The final, functional apparatus first came on line in 1999 and is depicted in Figure 1. What follows is a detailed description of the design, optimization, construction, validation, and application of this apparatus.

3. Components. 3.1. Design of Fluid Systems. 3.1.1. Reservoir. The reagent storage system was designed around a standard, 100-mL pear-shaped flask (Figure 2). To ensure that a wide range of materials including air- and moisture-sensitive reagents could be safely stored, the reservoir was designed to include a gas inlet that allowed the reservoir to be attached to a standard vacuum

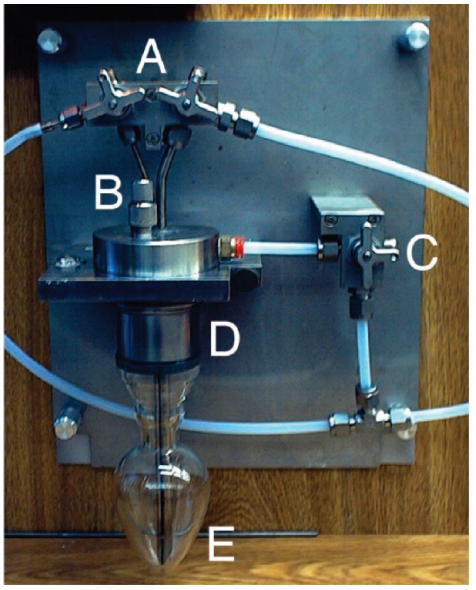

FIGURE 2. Close-up of the injectant reservoir. (A) Three-way valves controlling liquid and gas flow. Left line is for equilibration makeup, and right goes to the metering pump. (B) Cover to flask access port. (C) Gas inlet. Three-way valve allows gas to be sent into the reservoir flask or either line (for cleaning). (D) Kovar-to-glass union. (E) Reservoir flask and dip tubes.

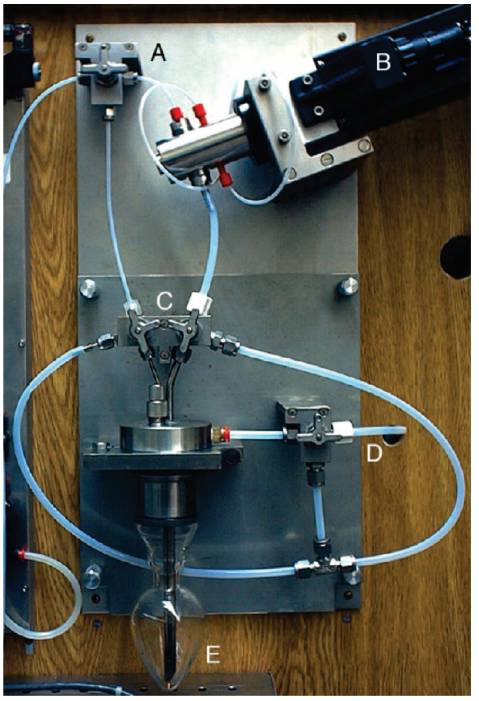

FIGURE 3. Close-up of the reservoir and Ivek metering piston pump. (A) Three-way valve to allow pumping or siphoning from the reservoir flask, E. (B) Metering pump. (C) Three-way valves that control liquid flow from the reservoir. (D) Inert gas inlet. (E) Reservoir flask and dip tubes.

manifold, and the headspace could be purged of oxygen and moisture using standard techniques. The reagent pickup lines, which feed into the metering system, were manufactured from stainless steel and extend into the bottom of the flask to ensure that a maximum of the solution stored in the reservoir could be used. Perhaps the most challenging part of designing the reservoir system was envisioning a safe and reliable method for attaching the glass flask to the stainless steel cap, which contains the gas inlet and solvent delivery lines. The final solution was to fit the flask with a glass-to-Kovar to stainless steel union. The necessary threads could then be carefully machined onto the stainless steel extension providing an airtight seal (O-ring) between the cap and flask. The entire reservoir system was mounted onto a brushed aluminum plate. The plate was then easily attached or removed from the RINMR cabinet, allowing the reservoir to be mobile without having to move the entire apparatus. This modular design allowed for easy cleaning and when necessary, a rapid exchange of different reservoirs. The gas and solvent lines connected to the reservoir were fitted with three-way valves to provide an easy shutoff and to allow for the solution to bypass the pump. The importance of this bypass will be discussed in detail below.

3.1.2. Injection Pump. The reservoir feeds directly to the metering pump, the first stage of the delivery system (Figure 3). Although the initial intent was to build the metering device, it quickly become apparent that it would be extremely difficult to manufacture a device that could accurately meter microliter quantities of a wide range of reagents. Instead, a third-party device was available that surpassed the design criteria.[12] Although the metering pump is available in various piston sizes, the largest piston was chosen for ease of priming. This system is quite flexible, allowing the selection of both the injection volume and the rate of injection.

3.1.3. Hydraulics. The most mechanically complex aspect of the RINMR apart from the metering pump is the reagent delivery system. In the resting position, the injector tip was located inside the NMR tube, ca. 20 mm above the solvent level. Injection requires the downward movement of the injector tip to the bottom of the NMR tube with simultaneous delivery of the reagent as the injector descends and as the solution and tube spin around it. Thus, two pneumatic actuators were installed to drive the injector tip into the solution and then return it to its resting position above the sample (Figure 4). The actuators were designed to operate separately so that the rates of downward and upward movement could be independently controlled.[13] Additionally, three optical sensors were installed: one at the upper end of travel (UEOT), one at the bottom end of travel (BEOT), and one in the middle. The middle optical sensor initiates the injection sequence for the downstroke. The BEOT optical sensor reverses the movement of the inject piston, while the UEOT optical sensor ends the process and sends an acquisition pulse to the spectrometer. The electronics control module allows for the injection to take place on either the down or upstroke. If upstroke is selected, the bottom optical sensor initiates the upstroke injection sequence, and the middle sensor is then rendered inactive. The whole of the operation is covered in detail in Section 3.2 (Design of the Electronic Control Module).

(12) *Digispense 2000* fitted with a size A alumina ceramic piston and an optional gland seal. The size A piston is rated from 1 to 2000 μL with 0.1 μL resolution. Contact IVEK Corp. at (800) 356−4746 or visit www.ivek.com.

(13) The rates of travel are controllable, but increasing or decreasing them too far can cause the pistons to not seat properly, leaving them in an intermediary position and unable to move without resetting them manually.

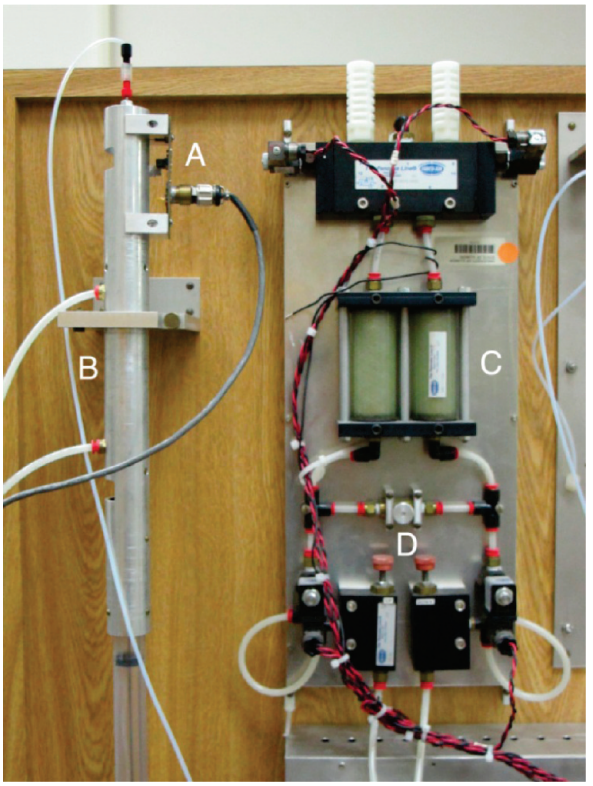

FIGURE 4. Pneumatic systems. (A) Electro-optical gates to control actuators. (B) Pneumatic piston location. (C) Pneumatic valve system. (D) Independent pressure adjustment controls for both the up and down strokes.

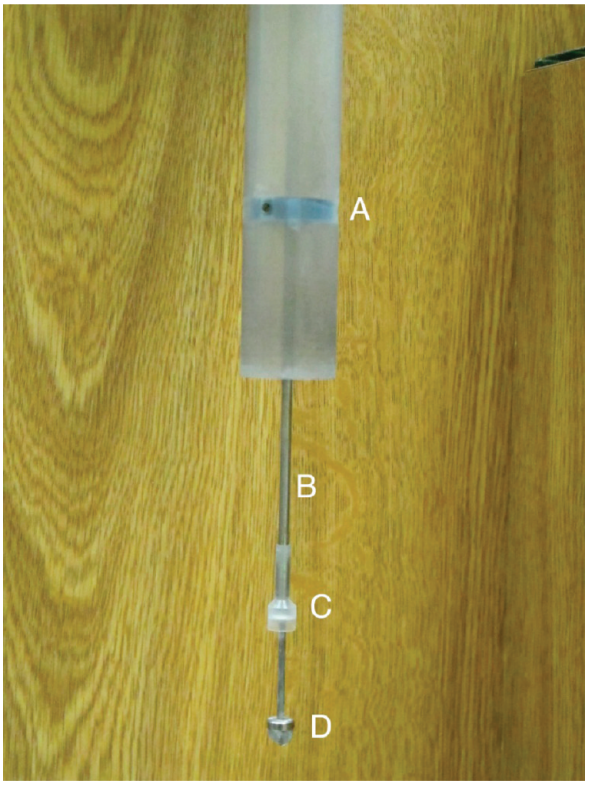

FIGURE 5. (A) Polycarbonate guide tube with spacer (black). (B) Outer titanium guide tube. (C) Kel-F sleeve. (D) Ten-millimeter injector tip, near full extension.

Although every care was taken to minimize the effects of a strong magnetic field on the RINMR apparatus, it was soon discovered that the NMR magnet could paralyze the actuators. Through trial and error, an operating distance of roughly 5−6 ft was found to be necessary to obviate the effects of the magnet.

3.1.4. Design of Injector. The injector tip and tube are manufactured from high-grade titanium,[14] which was chosen for its low magnetic susceptibility and chemical resilience.[15] The titanium injector tube is housed in a 1.04-m long high density polycarbonate tube fitted with guides to prevent accidental bending (Figure 5). The outer diameter of the guide tube is milled slightly smaller than the inner diameter of the upper stack and extends out above the magnet can. This tight fit and the internal guides are crucial in maintaining the trueness of the injector tube. Any curvature along the length of the titanium tube results in an off-axis movement of the injector tip leading to contact between the injector tip and the wall of the NMR tube during an injection cycle. In the best case, this contact slows the spin rate of the sample; in the worst case, this contact can shatter the tube.[16]

The pneumatic valve that actuates the injector mechanism is built directly onto the top of the guide tube and is physically connected to the titanium tube. The housing for the linear actuator is machined from aluminum and built to be wider than the spin stack, preventing the guide tube from contacting the sample spinner. Thus, the actuator housing rests at the very top of the spin stack and transfers the entire weight of the delivery apparatus to the magnet housing.

The injector must travel precisely down the center of the tube to ensure consistent rates of travel and tube spin. Because of the very tight tolerances inherent in this system, a physical alignment of the injector tube was needed to correct for deviations from trueness. In practice, the alignment of each new injector tube was checked before use and then periodically thereafter, especially if the exposed portion of the injector tube came into contact with anything during handling. This process was accomplished by placing the injector tube into an upper stack of the magnet in a custom-built stand discussed in section 4.3 and extending the injector tip until it was flush with the bottom of the stack. The alignment was then noted, and the injector tube was carefully bent by hand to compensate. This process was repeated until the injector was situated in the center of the opening at the bottom of the stack. Then, the alignment could be verified by placing an NMR tube in the stack. The tube was then spun at a constant rate and the injector was actuated. No change in the spin rate should be observed if the alignment is proper.

3.1.5. Evolution of the Injector Tip. Perhaps the most crucial and highly developed portion of the RINMR apparatus is the injector tip. During the initial period of development, the importance of proper tip design for accurate reagent delivery as well as for rapid mixing was not appreciated. Throughout the development process, each tip was milled from titanium

(14) Titanium tubing was made of A40 (< 0.04% iron), 0.083″ o.d., 0.063″ i.d., 60″ long.

(15) Although more costly and more difficult to machine than stainless steel or brass, initial testing with stainless steel tubing resulted in poor line shape, even at room temperature.

(16) In practice, small changes to this lateral alignment can be made manually as needed.

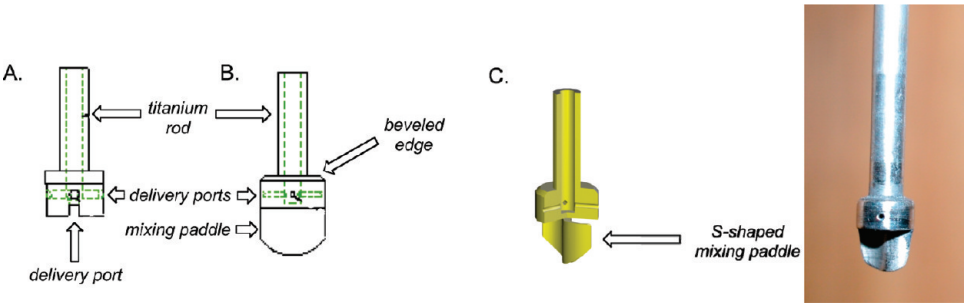

FIGURE 6. Several RINMR tip designs. (A) Intermediate design without mixing paddle. (B) Final design with mixing paddle. Note that the beveled edge allows for reseating inside the Kel-F sleeve. (C) Cutaway view of the final tip design and actual picture.

and then gold brazed onto the end of the titanium injector rod. In all, over 10 different tips were machined and tested. The designs were evaluated by metered injection of ethanol into a standardized solution of $CHCl_3$ in $CDCl_3$ at room temperature and if successful, then again at −60 °C. The level of mixing efficiency was determined by comparison of ^1H integrations after a single injection and then after shaking the NMR tube. The initial design consisted of a simple flared circular tip with a single delivery port at the bottom (Figure 6). Evaluation of this design revealed accurate delivery albeit extremely poor mixing efficiency after a single injection. To improve mixing, the single port was modified to three delivery ports each 0.025 mm (0.010″) in diameter spaced radially at 120° around the waist of the tip. A Teflon cap was also added to cover the ports to minimize the effects of diffusion during equilibration. It was believed that the cap would slip down and away from the tip during fluid delivery. Although the results improved somewhat, the mixing efficiency was by no means ideal, and it was quickly discovered that the amount of fluid delivered was not sufficient to create enough pressure to remove the Teflon cap. In a subsequent design, a fourth delivery port was added to the bottom of the tip to redistribute the pressure on the cap. The results were a significant improvement in mixing efficiency at room temperature. However, in the final design, an S-shaped mixing paddle was added to the bottom of the tip containing three radially spaced delivery ports. The Teflon cap was replaced with a Teflon sleeve attached to the guide tube that fitted around the ports to provide a seal during setup and equilibration. When delivering reagent, the tip slides down and away from the stationary sleeve and then resets back inside the sleeve at the end of the injection cycle. Evaluation of this design showed excellent mixing efficiency at room temperature. Surprisingly, similar tests at −60 °C resulted in little or no delivery of ethanol. Further testing confirmed that equilibration of the injector assembly at subambient temperatures resulted in the contraction of the solvent up the injector tip as it cooled. To prevent this, a separate line was connected to the delivery line, bypassing the metering pump.[17] This "make-up" line was attached to the delivery line via a 3-way valve and allowed for fluid to be directly removed from the reservoir during equilibration. Although Teflon was initially used for the injector tip sleeve, its pliability forced the use of new sleeves after only 4 or 5 injections. Kel-F was found to be a superior

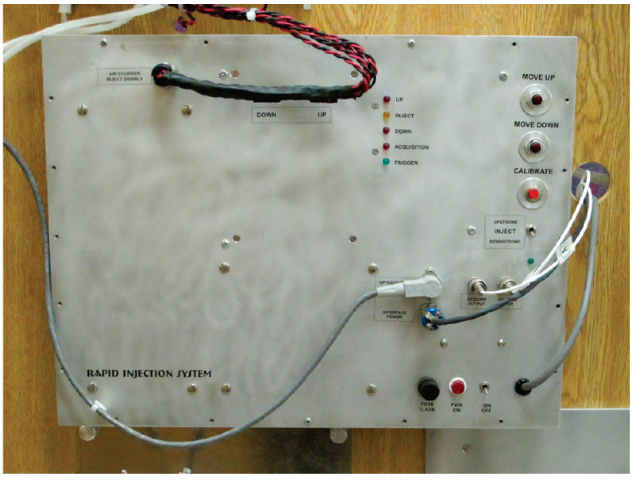

FIGURE 7. Electronic control module (ECM).

replacement to Teflon, lasting nearly 100 cycles before requiring replacement. With the tip, sleeve, and makeup line in place, fluid could be routinely delivered with excellent mixing over a broad temperature range.

Although the Kel-F sleeve effectively limited atmospheric exposure, proper cleaning (rinsing with solvents used, followed by abs EtOH, and rigorous air drying) is required. Over time, the tip can become clogged, and sonication while pulling a vacuum on the interior of the injector tube was effective in clearing clogged ports.[18] It should be noted that hundreds of injections have been run with solutions containing $SiCl_4$ (which gives SiO_2 upon hydrolysis) before this rigorous cleaning was necessary when the injector was properly rinsed after use.

3.2. Design of the Electronic Control Module. The signals necessary to operate the linear actuator and the Ivek fluid pump are generated in the electronic control module (ECM, Figure 7) whose design is illustrated as a block diagram in Figure 8. The process begins with a trigger pulse generated by the spectrometer (from a BNC connector labeled SP1 on the back of the Inova equipment console). This trigger pulse (T) is sent through a coaxial cable to an INPUT TRIGGER BUFFER located in the ECM. The buffer generates a local trigger that is generated either by the spectrometer pulse or by a button on the ECM (labeled "calibrate"). This button allows for local initiation of the inject procedure for purposes of calibrating inject volumes, linear actuator speeds, or cleaning

(17) Later designs also required a slight modification: A small amount of the inside of the sleeve was removed to compensate for the braise point where the tip was attached to the injector tube.

(18) The wires used for cleaning microliter syringes can also be useful in clearing clogged ports.

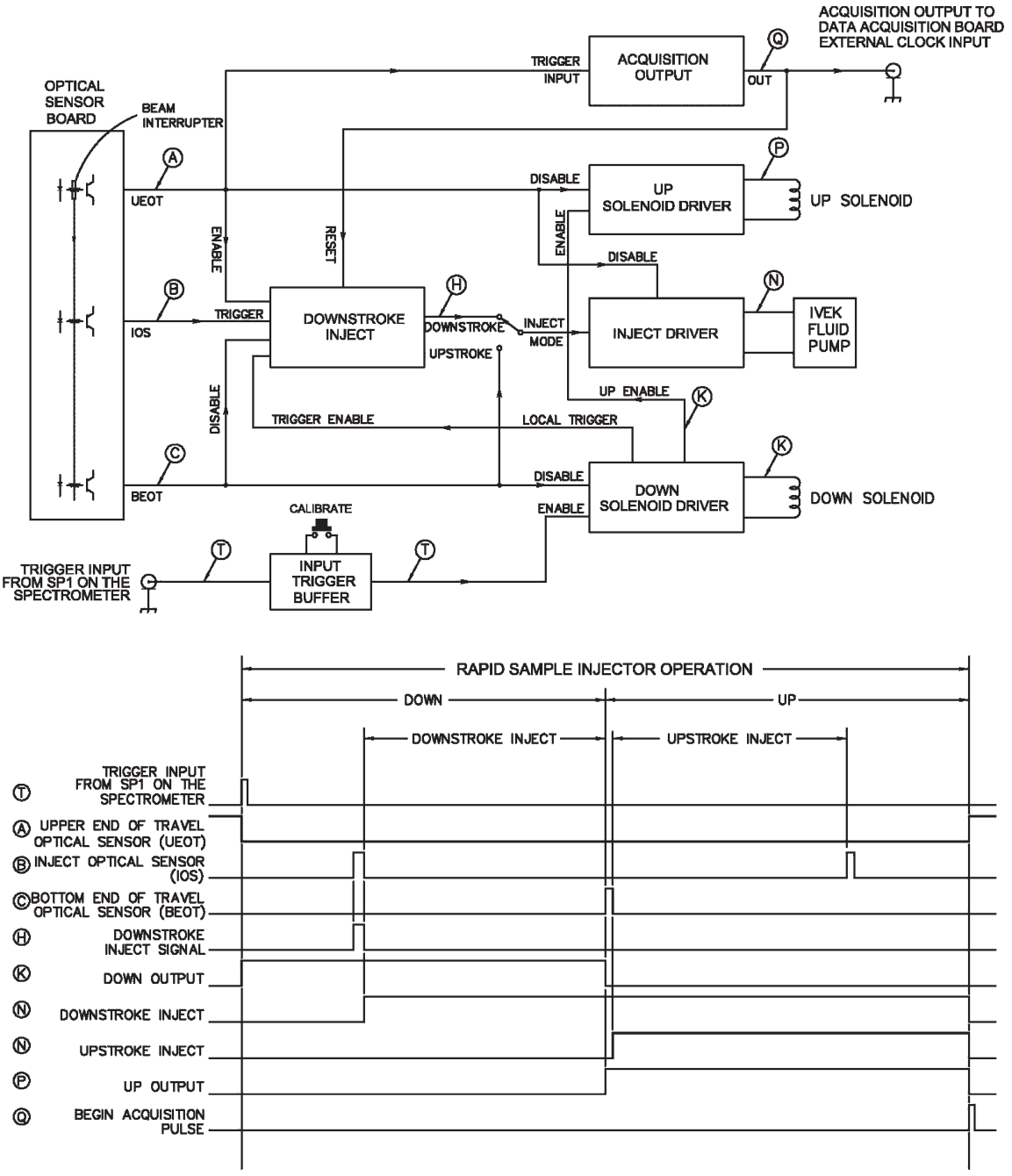

FIGURE 8. Wiring diagram (A) and waveforms (B) for the electronic control module.

the system tubing. The trigger pulse then goes to the DOWN SOLENOID DRIVER (DSD), which starts the linear actuator moving down at velocity v_{down} (waveform K). The speed of this velocity is controlled by a valve located between the gas source and the linear actuator, which has a thumb-screw adjustment (Figure 4) for effecting changes to v_{down}.

Three optical sensors are located at the top of the sample inject tube (Figure 1A). These sensors consist of a light-emitting diode (LED) shining on a phototransistor across a gap that allows the beam to be interrupted, thus turning the phototransistor on or off. These sensors are mounted on a circuit board that remains fixed while the beam interrupter, which is attached to the linear actuator, moves through the gap between the LED and the phototransistor. The top sensor is called the upper end of travel (UEOT) optical sensor and senses when the actuator is at the upper end of travel. Initially, the UEOT phototransistor is turned off as the beam interrupter is resting in the UEOT gap. As the linear actuator begins its travel downward, the beam interrupter moves out of the gap, which causes the phototransistor to turn on and waveform A to go from high to low.

The beam interrupter then approaches the inject optical sensor (IOS) causing waveform B to go from low to high and back to low again as the beam interrupter passes through. This pulse is sent to the DOWNSTROKE INJECT LOGIC's "trigger" input that generates waveform H. If the INJECT MODE switch on the front panel of the ECM is set for downstroke inject, waveform H is sent to the INJECT DRIVER's "begin inject" input

to begin the inject sequence (waveform N_{down}). The volume of the fluid injection and the rate at which it is delivered are controlled by the Ivek pump controller, which is a separate unit. There are UP/DOWN timers on the ECM that individually time the up and down stroke. This helps facilitate the setting for the fluid injection rate on the Ivek pump.

The beam interrupter then arrives at the bottom end of travel (BEOT) optical sensor causing waveform C to go from low to high. This simultaneously disables the DSD and enables the UP SOLENOID DRIVER (USD, waveform K going from high to low and waveform P going from low to high) causing the linear actuator to instantly reverse direction and waveform C to go from high to low. At this point the injection is finished. As the linear actuator begins its upward travel at velocity v_{up}, controlled by a valve similar to that for v_{down} shown in Figure 4, mixing by the S-shaped paddle located on the injector tip (Figure 6) begins in earnest. The pulse generated at waveform C disables the DOWNSTROKE INJECT LOGIC, so that it cannot send an inject pulse as the beam interrupter passes through the IOS on the return trip to the UEOT. (Waveform C is also sent to the INJECT MODE switch. If the INJECT MODE switch on the front panel of the ECM is set for upstroke inject, the DOWNSTROKE INJECT LOGIC is bypassed, and waveform C is sent to the INJECT DRIVER to begin the inject sequence, waveform N_{up}.)

The beam interrupter then arrives at the UEOT optical sensor causing waveform A to go from low to high. This then disables both the USD and the INJECT DRIVER. Waveform A is also sent to the ACQUISITION OUTPUT's "acquisition trigger" input. This new trigger, generated by the ACQUISITION OUTPUT LOGIC, is then sent to the "external clock" input on the DATA ACQUISITION BOARD of the spectrometer via a coaxial cable (waveform Q). At this point the rapid sample inject sequence is complete. The spectrometer then resumes the experiment and the acquisition process begins.

4. Validation and Calibration. 4.1. Volume. Initial injection volume calibrations were performed outside of the magnet by injecting a solution of ethanol in $CDCl_3$ into a solution of dichloromethane in $CDCl_3$ at room temperature. The samples were mixed, the integrated NMR spectra of these samples were acquired, and the integral data was compared. Once assured that the metering pump was accurately and reproducibly delivering the desired amount of solution under nominal conditions, the volume calibrations were repeated at −60 °C inside the magnet, and integrals were measured repeatedly over ca. 1 min after injection. The samples were then removed from the magnet and shaken, and the NMR data were reacquired. Unfortunately, this comparison showed that the samples had to be shaken before the correct integral values were obtained. This disparity indicated that the metering pump was delivering the appropriate volumes but that inadequate mixing was occurring inside the magnet. This solution to this problem is described in Section 4.3 (Mixing).

After optimization of the injection sequence to provide a homogeneous sample (see below), the volume calibration was repeated in quadruplicate at −60 °C inside the magnet, and the integration data were again compared (Figure 9). The comparison of the measured to injected volumes was linear as expected, and the data was stable over ca. 1 min. Thus, the desired volumes of injectant were being accurately and reproducibly delivered to the sample tube, and mixing was complete and rapid.

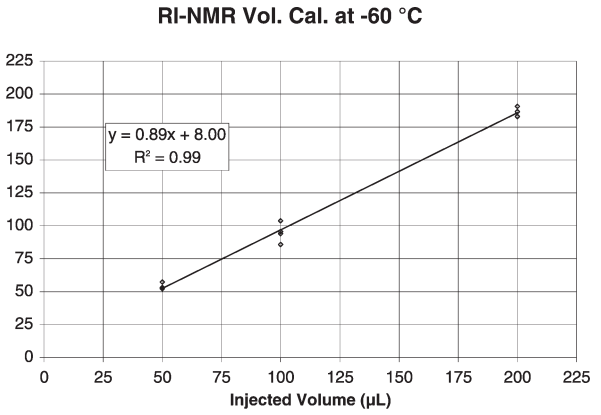

FIGURE 9. Plot of the measured injection volume vs the volume selected for injection.

4.2. Temperature. A variety of temperature parameters were studied. First, the thermocouple in the probe was calibrated against a standard Varian methanol temperature calibration standard to ensure the accuracy of the readings. Next, the temperature gradient needed to be considered. While the temperature at the thermocouple was controlled at −70 °C, the temperature farther from the thermocouple was uncertain. To understand the change in temperature gradient up the stack, a thermocouple was inserted into the probe through the guide tube. The temperature at various locations could then be measured by varying the position of this thermocouple. Placing this thermocouple at the location of the injector tip above a sample that was maintained at −70 °C revealed a temperature ca. 10 °C warmer, even over this short distance (ca. 50 mm). Cooling gas flows were increased to 20 L/min to minimize the gradient. It should be noted that even with a 10 °C difference in temperature, a typical injection would increase the sample temperature by less than 1 °C.

4.3. Mixing. Whereas injecting a given volume rapidly and reproducibly was straightforward to achieve, creating a homogeneous sample thereafter proved more difficult. Initial calibration runs demonstrated that injection did not give a homogeneous solution, and integral values tended to drift with time after the injection as further (slow) mixing occurred. To solve this problem required direct observation of the mixing process. Thus, to facilitate this evaluation, a stand was constructed for the upper stack of the instrument so that an injection into a spinning sample outside the magnet could be accomplished and the results observed visually (Figure 10). Because injections of a colored dye solution occurred too rapidly to evaluate with the unaided eye, high-resolution video recording was required. Video data collected from each run could then be inspected in slow-motion to observe the course of the injection and the adequacy of sample mixing. Some freeze-frame images acquired during this process can be seen in Figure 11, and a sampling of the video clips is included in the Supporting Information.

A problem that was discovered while analyzing the video data is a delay in the onset of injection. The inject optical sensor (IOS, Section 3.2) was positioned to actuate the Ivek metering pump just as the injector tip reached the top of the liquid in the NMR tube. However, for unknown reasons, the delivery of reagent was delayed, resulting in a concentration gradient at the bottom of the tube. The video data showed

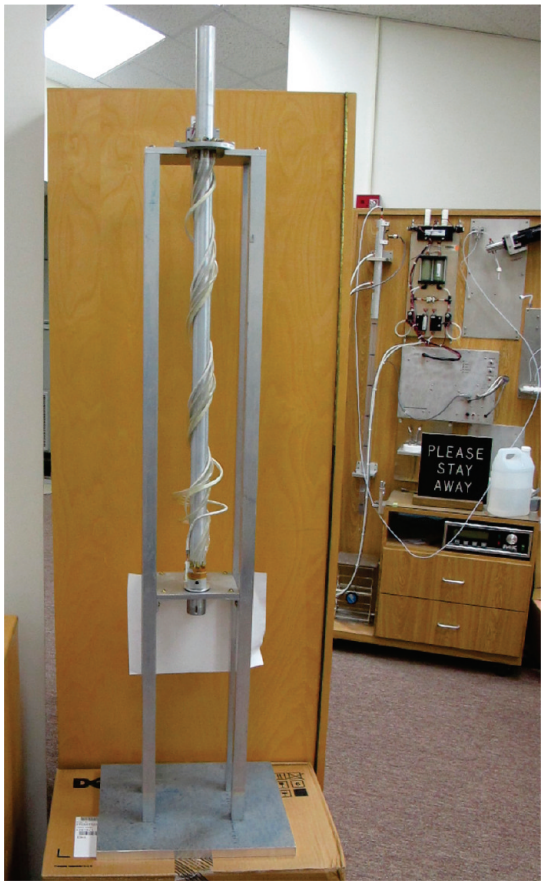

FIGURE 10. Stand manufactured to hold the upper stack and allow visual inspection of the injection process. The RINMR instrument is in storage configuration in the background. The injector is stored upright to minimize warping along the length of the titanium injector tube.

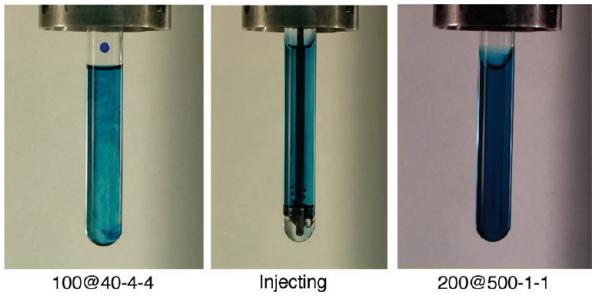

FIGURE 11. Examples of poor (left) and good (right) mixing of an injected dye solution into 10-mm (bottom) NMR tubes. The center image shows the injector tip near full extension. Numbers below each frame illustrate the injection program used: total injection volume (μL) at injection rate (μL/s)−no. of seconds to travel down−no. of seconds to travel up. Center and right-hand samples were spun at 20 Hz. Left-hand sample was not spun to illustrate the added mixing that occurs when the spinning sample encounters the s-shaped paddle on the bottom of the injector.

that the mixing paddle effectively distributed the gradient, but to ensure homogeneity, the timing of the injection was advanced such that the pump was actuated slightly before the tip entered the solution in the sample tube.

The RINMR system has some limitations with respect to mixing speed, some of which are related to the technique, and some of which are specific to the instrument. For example, the time required to create a homogeneous sample in a 5-mm NMR tube is longer than that in a 10-mm tube, which became apparent when attempting to sample at ca. 3 s intervals using a 5-mm tube. Additionally, the injection cycle for 10-mm tubes was optimized at a total time of 4 s. This parameter limits how rapidly the first data point can be collected to about 3 s after the beginning of the injection.

5. Data Acquisition and Manipulation. A standard Varian pulse sequence (s2pul) was modified to include the production of a trigger pulse sent to the ECM and to wait for a trigger pulse from the ECM before beginning the acquisition (see Section 3.2 above). A conditional statement was included so that this exchange of triggers occurred only prior to acquisition of the first spectrum of the arrayed set. Acquisition parameters were modified to obtain quantitative integral data. Namely, 90° pulse widths and T_1 times were determined. The pulse width was set to 22.5°, 45°, or 90°, and the recycle delay time was set to 3−5 times the longest T_1 time (3× for 22.5°, 4× for 45°, and 5× for a 90° pulse). A paramagnetic relaxation agent (such as $Cr(dpm)_3$) can be added to decrease the T_1 relaxation times. In general, acquiring data in a quantitative manner slows data acquisition and only needs to be done when quantification is required. Qualitative data can be acquired much more rapidly.

Data sets were acquired as arrayed experiments. This protocol facilitated data storage and manipulation by creating a single file that could be processed as a group. That is, one spectrum could be phased, line broadened, and integrated, and then these properties could be propagated to all of the spectra from the experiment. Once the data was collected, a spectrum would be phased, the appropriate peaks would be integrated to at least ±2.5 times the line width to ensure the integral region contained all of the signal intensity and, in some cases, baseline-corrected. In some cases, each spectrum would be phased independently. Changes in phase with time was not uncommon and could be corrected for. In practice, a number of different workup scripts were written so that they could be called in rapid succession to determine which parameters needed to be adjusted to control phase and baseline drift and give accurate integral values. These scripts also automated retrieval and tabulation of integral data into a format that could be easily imported into a spreadsheet program for plotting and further analysis.

6. Reliability. It should be noted that over the course of this instrument's lifetime (now ca. 12 years) no probe has been damaged, no instrument time has been lost, and not even a single sample tube has been broken in the magnet. This record is a testament to the tight design tolerances and the reliability in use this instrument demonstrates.

7. Implementation. 7.1. Trichlorosilyl Enol Ether Kinetics. Previous publications from these laboratories illustrated the utility of chiral Lewis base catalysis in asymmetric aldol additions of trichlorosilyl enol ethers.[19] For example, the combination of cyclohexanone trichlorosilyl enol ether (**1**) with benzaldehyde (**2**) in the presence of chiral phosphoramides (Scheme 1) affords aldol products with high diastereoselectivities and moderate to high enantioselectivities. During the

(19) (a) Denmark, S. E.; Fujimori, S. In *Modern Aldol Reactions*; Mahrwald, R., Ed.; Wiley-VCH: Weinheim, 2004; Vol. 2. Chapter 7. (b) Denmark, S. E.; Stavenger, R. A. *Acc. Chem. Res.* **2000**, *33*, 432–440. (c) Denmark, S. E.; Fujimori, S.; Pham, S. M. *J. Org. Chem.* **2005**, *70*, 10823–10840.

TABLE 1. Arrhenius Activation Energies for Aldol Additions of Trichlorosilyl Enol Ethers Determined by ReactIR and RINMR Analysis[a]

conditions	method	E_a (kcal mol^{-1})	A (M^{-1} s^{-1})	$\Delta H^{\ddagger}$ (kcal mol^{-1})	$\Delta S^{\ddagger}$ (cal mol^{-1} K^{-1})	$\Delta G^{\ddagger}$ (kcal mol^{-1})
1 + **2**, 5 mol % **5**	ReactIR	0.9 ± 0.1	5.1 ± 1.7	0.3 ± 0.1	−67.1 ± 0.7	20.6 ± 0.2
1 + **2**, 5 mol % **5**	RINMR	1.8	0.4	1.2	−63.3	20.4
1 + **2**, 10 mol % **4**	RINMR	2.1 ± 0.5	224 ± 100	1.5 ± 0.5	−51.9 ± 1.0	17.3 ± 1.0

[a]Activation parameters were calculated for T = 303 K.

course of optimization it was discovered that the diastereoselectivity of the aldol addition is highly sensitive to the bulkiness and loading of the catalyst. To explain this behavior, a mechanistic rationale was formulated in which the reaction proceeds through independent pathways to the two diastereomers, such that the operative pathway is dependent upon catalyst size and concentration. The central tenet of this hypothesis is that the two pathways differed in the number of catalyst molecules in the rate- and stereochemistry-determining transition structures. Thus, pathways involving either one or two phosphoramides are available, the former being operative with bulky catalysts or low catalyst concentration, to afford *syn*-adducts from **1**, whereas the latter is operative with less sterically encumbered catalysts and higher catalyst concentrations to give *anti*-adducts. To differentiate these two pathways and validate the hypothesis, a series of kinetic studies were undertaken.[20]

SCHEME 1

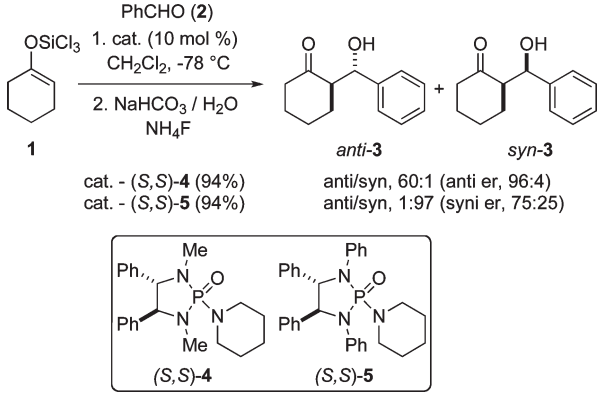

Initial efforts using simple GC analysis and ReactIR techniques were successful in studying the addition of **1** to **2** catalyzed by phosphoramide **5** and clearly established *first*-order dependence on [**1**], [**2**], and [**5**]. Unfortunately, similar studies using phosphoramide **4** were inconclusive because of limited instrument sensitivity and the enhanced rates afforded by this catalyst. To overcome these obstacles, the RINMR instrument offered the opportunity to secure more accurate kinetic measurements. To validate the utility of the newly constructed RINMR, the addition of **1** to **2** catalyzed by **5** (previously studied by *in situ* IR methods) was reexamined. These experiments were performed in a 5-mm NMR tube containing enol ether **1** and the phosphoramide in CD_2Cl_2. Benzaldehyde (**2**) was added via the injector as a solution in CD_2Cl_2 solution. In general, a ^{1}H NMR spectrum was acquired immediately prior to injection to ensure that no leakage had occurred. Data points were then rapidly recorded following injection of the desired amount of **2**. Experiments were generally conducted in triplicate to ensure reproducibility. Using this protocol, Arrhenius parameters were determined over a temperature range of −11 to −65 °C. RINMR analysis provided good agreement with the previous IR studies, Table 1.[21]

Thus secured, the more challenging task of studying reactions promoted using the more reactive phosphoramide **4** was undertaken. To determine the order in catalyst, the rate of the aldol addition between **1** and **2** was measured as a function of the concentration of **4**. Injections were performed at −80 °C using a 10-fold range in catalyst concentration. Data points were collected at 1-s intervals for no less than five half-lives. Plotting the data as log(k_{obs}) vs log([catalyst]) revealed a *second*-order dependence (m = 2.113) on phosphoramide **4**, Figure 12. This provided the direct evidence for a mechanistic dichotomy between catalyst **4** and **5**, namely, that reactions using **4** proceed through a two phosphoramide pathway whereas reactions using **5** proceed through a one phosphoramide pathway. On the basis of these results, two different rate equations could be formulated:

$$\frac{d(\mathbf{3})}{dt} = k[\text{enol ether}][\text{aldehyde}][\mathbf{4}]^2$$

and

$$\frac{d(\mathbf{3})}{dt} = k[\text{enol ether}][\text{aldehyde}][\mathbf{5}]$$

Arrhenius parameters were also determined using 10 mol % **4** over a 20 °C temperature range, between −70 and −90 °C, Table 1. Attempts to extend this temperature range while maintaining CD_2Cl_2 as the bulk solvent proved unsuccessful because of extremely fast reaction rates for temperatures above −65 °C. Conversely, decreasing the temperature below −90 °C resulted in highly viscous solutions and presented the possible risk of sample freezing. Comparing the Arrhenius activation parameters for the two catalyzed reactions shows a remarkable dependence of $\Delta G^{\ddagger}$ on $\Delta S^{\ddagger}$. Reactions with high entropic costs are often rationalized by virtue of a highly

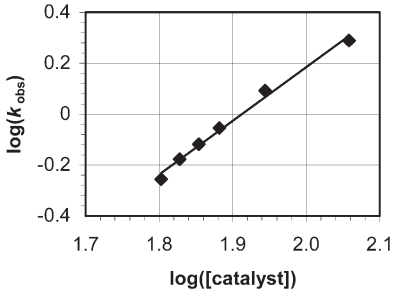

FIGURE 12. Plot of log(k_{obs}) vs log([catalyst]) for the addition of **1** to benzaldehyde catalyzed by **4** at T = −80 °C. The graph depicts the linear fit to $f(x) = mx + b$ (m = 2.113, R^2 = 0.992).

(20) (a) Denmark, S. E.; Pham, S. M. *Helv. Chim. Acta* **2000**, *83*, 1846–1853. (b) Denmark, S. E.; Pham, S. M.; Stavenger, R. A.; Su, X.; Wong, K. T.; Nishigaichi, Y. *J. Org. Chem.* **2006**, *71*, 3904–3922.

ordered transition structure or a highly unfavorable preequilibrium. In the case involving these aldol additions, one or both of these may be operative.

Thus, RINMR kinetics unambiguously determined a second-order dependence for aldol reactions with phosphoramide **4** and a remarkable entropic dependence on $\Delta G^{\ddagger}$ for these reactions. It is also interesting to note that the preparative results indicate that the reactions involving catalyst **4** are more enantioselective as compared to phosphoramide **5**, suggesting that the 2:1 (phosphoramide/silicon) pathway is more discriminating. To observe the enhanced stereoselectivity of the active 2:1 complex, one must also conclude that the 2:1 complex is more kinetically viable than the 1:1 complex. From a mechanistic standpoint, reaction through the 1:1 pathway should only be available when the 2:1 pathway is inaccessible. If so, increasing the local concentration of the second Lewis basic unit should greatly enhance the 2:1 pathway over the less desirable 1:1 pathway. These conclusions led to the formulation of highly active and selective bisphosphoramides as catalysts for the aldol additions of silyl enol ethers derived from aldehydes, ketones, esters, nitriles, and conjugated ketones, esters, and amides to aldehydes.

7.2. Propionate Silyl Ketene Acetal Aldol Kinetics. A long-standing question in Lewis base catalyzed aldol additions is the mechanism of Lewis base activation of the weak Lewis acid, $SiCl_4$. Empirically, the combination of a Lewis base with a weak Lewis acid led to rapid and highly selective addition of silyl ketene acetals to aldehydes (e.g., Scheme 2). A typical preparative reaction is complete within minutes at −78 °C, necessitating the utmost rapidity in data collection to ensure accurate kinetic data. As an example, Figure 13 shows a typical data set from a kinetic analysis of the reaction shown in Scheme 2. Inspection of the data in Figure 13 demonstrates the versatility of the technique: both the disappearance of **7** and the appearance of **8** can be tracked. No intermediates are formed over the course of the reaction, indicated by the lack of any transient signals in the NMR spectrum over time.

SCHEME 2

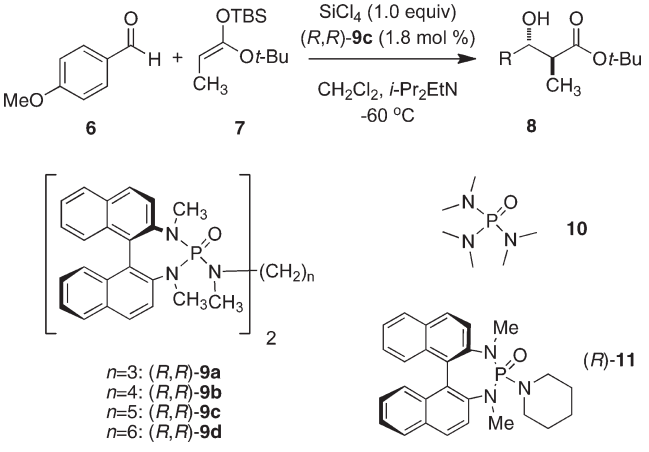

A full kinetic analysis of the Lewis base catalyzed aldol addition was recently published.[4a] The study of this system proved to be an extraordinarily practical showcase for this instrument; a full kinetic analysis of this system with a number of different catalyst systems demonstrated the instrument's exquisite ability to collect meaningful kinetic data at cryogenic temperatures with air-sensitive reagents.

The basics of this reaction are quite simple. The reaction displays partial first-order kinetics in both aldehyde and silyl ketene acetal, as expected for a simple aldol addition reaction. Control experiments showed no rate dependence upon the concentrations of the added acid scavenger (DIPEA) or upon the added paramagnetic relaxation agent [$Cr(dpm)_3$]. All of the systems studied also showed zero-order kinetics with respect to $SiCl_4$ concentration. While at first glance this is counterintuitive, it simply illustrates that the actual catalytic species is in fact the Lewis acid−Lewis base complex. Because the Lewis base is catalytic and the Lewis acid is used in stoichiometric quantities, the quantity of the complex in solution is defined only by the concentration of the Lewis base.

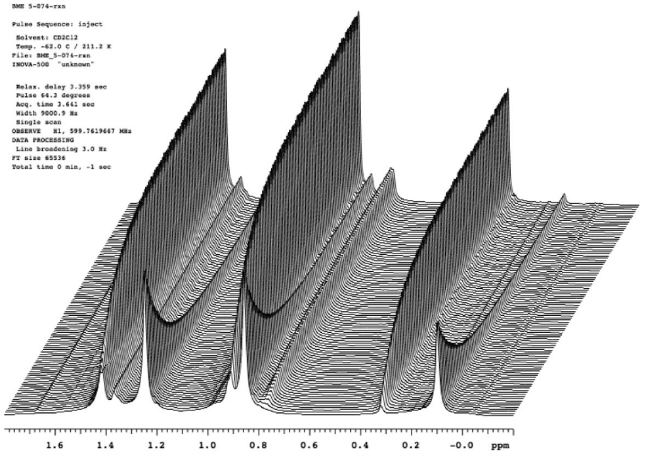

FIGURE 13. Aliphatic region of the reaction of **6** and **7** in the presence of $SiCl_4$ and catalyst **9c**. Spectra were recorded every 7 s for ca. 30 min. In this example, the reaction $t_{1/2}$ is ca. 3 min.

Of greater interest were the striking differences in the catalytic Lewis base partial reaction orders. The hypothetical catalytic cycle, drawn by analogy to the Lewis base catalyzed allylation reaction, proposed a 2:1 Lewis base to Lewis acid complex as the active catalyst system (Scheme 3).[22] According to this hypothesis, monodentate phosphoramides (cf., **10**, **11**) would display second-order partial rates, while the bidentate phosphoramides would display first-order kinetics. To our surprise, the actual partial rate data was much more complex, pointing to the more complex nature of the catalyst resting state.

The monomeric catalyst **11** displayed a first-order partial rate dependence, whereas HMPA (**10**) displayed a complex 2/3 partial order, each different from the expected second-order behavior. It is a testament to the reproducibility and sensitivity of the instrument that first and 2/3 partial reaction orders could be accurately differentiated.

The dimeric catalysts **9a** and **9b** each display partial first-order kinetic behavior, as expected. However, dimeric catalysts **9c** and **9d** displayed 1/2 order kinetic behavior, when

(21) The RINMR numbers for **5** are a single measurement and therefore do not include quantified errors. Nevertheless, all of the energy parameters (E_a, $\Delta H^{\ddagger}$, and $\Delta G^{\ddagger}$) differ from the accepted ReactIR numbers by less than 1 kcal/mol.

(22) For a summary see: Denmark, S. E.; Eklov, B. M.; Yao, P. J.; Eastgate, M. D. *J. Am. Chem. Soc.* **2009**, *131*, 11770–11787. and references therein.

SCHEME 3

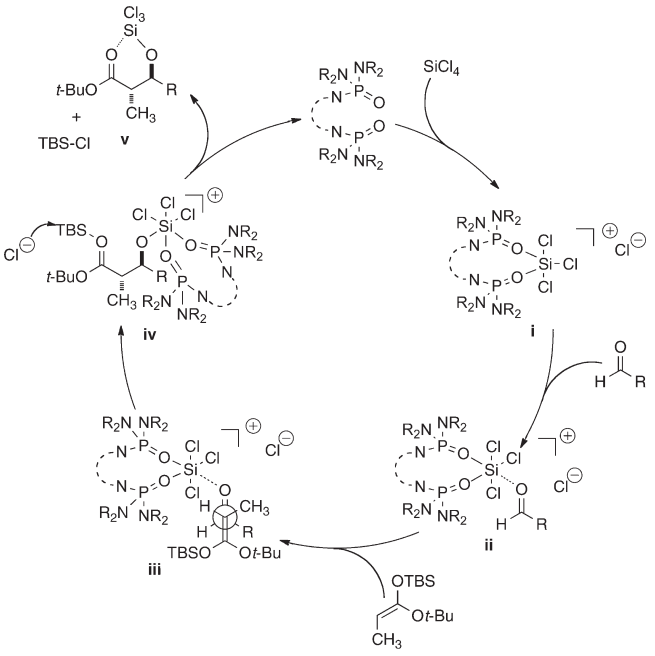

SCHEME 4

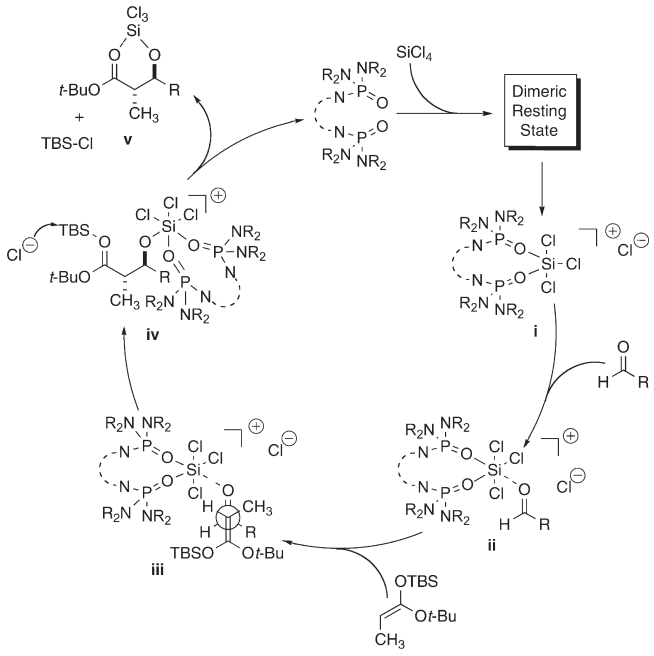

these were also expected to display first-order rate dependencies. These four catalysts differ only in the length of the alkyl linker separating the two phosphoramide units. The fact that varying the length of the tether was changing the partial reaction order of the catalyst was very surprising to say the least.

The exquisite granularity of this data allowed the derivation of a unified reaction mechanism that is consistent with all of these different catalyst behaviors (Scheme 4). The data is consistent with the earlier proposed 2:1 Lewis base to Lewis acid complex as the active catalyst in all of these systems. It is the nature of the catalyst resting states that required modification. For the simplest catalyst, **11**, this resting state is a 2:1 complex, as a mixture of neutral and cationic species. Because the 2:1 complex is already formed in the resting state, no additional **11** is required to reach the transition state, and a first-order rate is observed. The same 2:1 complex is required in the transition state with HMPA, but in this case the resting state is a 3:1 complex.[3a] The observed 2/3 order rate dependence demonstrates that one of the three HMPA must dissociate from the complex before reaching the transition state.[23] The dimeric catalysts **9a** and **9b** are readily explained by our original hypothesis: these phosphoramides are bidentate in both the ground and transition states and hence display partial first-order rate dependencies. Dimeric catalysts **9c** and **9d** both displayed 1/2 order partial rates. By postulating that the same intermediate is involved for all four of the dimeric phosphoramides **9a**−**d**, the 1/2 order rate demands a dimeric resting state. The longer tethers in **9c** and **9d** allow these phosphoramides to bridge between two silicon atoms and form large macrocyclic resting states, which then break down to form two active catalysts. The proposed resting states discussed above have all been supported by spectroscopic observations (^{29}Si and ^{31}P NMR), and the large macrocyclic dimers are precedented.[4a]

(23) In other words, the order in HMPA is the ratio of the molecularity in the transition state divided by the molecularity in the ground state.

7.3. *meso* Epoxide Opening Kinetics. The advantages of rapid injection NMR as a noninvasive technique for the study of reaction kinetics are nicely illustrated in the case of the Lewis base catalyzed opening of *meso* epoxides with silicon tetrachloride ($SiCl_4$). An earlier publication from these laboratories had shown that the chiral phosphoramide **3** gives good yields and enantioselectivities in the desymmetrization process with a range of *meso* epoxides (Scheme 5).[24] Since then, a variety of diverse catalyst structures including *n*-oxides[25] and phosphine oxides[26] have been disclosed that promote this transformation, but few have achieved significant improvements in terms of scope or selectivity. To further understand the catalytic process and find a logical path forward for optimizing selectivity with these phosphoramide-containing catalysts, kinetic studies were needed to elucidate the mechanism of the reaction and understand the role of the catalyst. Unfortunately, the rapid rate and moisture sensitivity of this reaction make it an extremely difficult case for traditional analytical techniques. Sampling by syringe for high performance liquid chromatography (HPLC) or gas chromatography (GC) would allow the aliquot to rapidly warm to room temperature, leading to results that are not representative of the true state of the reaction at −78 °C. Furthermore, removing an aliquot by syringe could lead to hydrolysis of $SiCl_4$, opening a competitive and unselective Brønsted acid catalyzed pathway and further complicating analysis.

Initial attempts to monitor the reaction using *in situ* infrared spectroscopy as a noninvasive technique did address the precision and reproducibility issues associated with HPLC

(24) Denmark, S. E.; Barsanti, P. A.; Wong, K.-T.; Stavenger, R. A. *J. Org. Chem.* **1998**, *63*, 2428–2429.

(25) (a) Tao, B.; Lo, M.-C.; Fu, G. C. *J. Am. Chem. Soc.* **2001**, *123*, 353–354. (b) Nakajima, M.; Saito, M.; Uemura, M.; Hashimoto, S. *Tetrahedron Lett.* **2002**, *43*, 8827–8829. (c) Malkov, A. V.; Gordon, M. R.; Stončius, S.; Mussain, J.; Kočovsky, P. *Org. Lett.* **2009**, *11*, 5390–5393.

(26) (a) Tokuoka, E.; Kotani, S.; Matsunaga, H.; Ishizuka, T.; Hashimoto, S.; Nakajima, M. *Tetrahedron: Asymmetry* **2005**, *16*, 2391–2392. (b) Pu, X.; Qi, X.; Ready, J. M. *J. Am. Chem. Soc.* **2009**, *131*, 10364–10365.

SCHEME 5

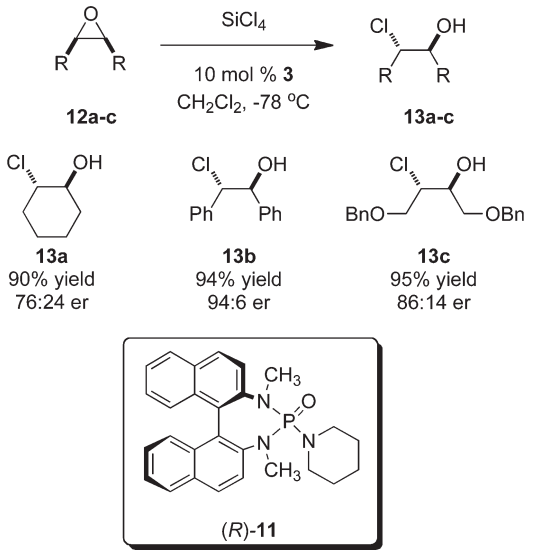

and GC monitoring. However, because no strong IR absorbance was available in the molecule of interest, only the weak absorbance of the C−O bond in the epoxide could be used. In the end, this technique proved unreliable because of signal overlap, and these studies were abandoned.

By comparison, RINMR was a more promising technique for this study because it represents a noninvasive technique that can detect more diagnostic signals for these structures. Initial experiments confirmed that the high levels of signal dispersion accessible on a 500 MHz (^{1}H) NMR instrument would allow for accurate monitoring of reaction conversion without the kind of problems associated with signal overlap encountered with ReactIR.

Having confirmed the viability of this method, the kinetic experiments were performed in a 10-mm NMR tube with a solution of 1.1 equiv of $SiCl_4$ and HMPA as catalyst in CD_2Cl_2 at −75 °C (Scheme 6).[27] The epoxide **12b** was then added from the injector as a solution in $CDCl_3$, generating a solution with an overall concentration of 0.2 M. First, the order of each reagent was determined using the integral method with initial rate analysis.[28] Each data point was reproduced in triplicate. Minor variations between runs were observed, likely due to a competitive Brønsted acid catalyzed pathway, but the data was sufficiently reliable to draw some important conclusions regarding the reaction mechanism.

Employing the integral method to analyze the raw data revealed that the reaction exhibited good, overall first-order behavior (Figure 14A and B). Overall second-order behavior was ruled out by comparison of graphs of ln(**12b**$_t$) and 1/(**12b**$_t$) versus time out to 70% conversion (R^2(ln(**12b**$_t$)) = 0.9977 vs R^2(1/(**12b**$_t$)) = 0.9421). The linearity of the ln(**12b**) versus time plot was clearly higher than that of the 1/(**12b**) versus time plot (Figure 14C). A similar conclusion could be drawn from plots of ln(1 − **13b**$_t$) and 1/(1 − **13b**$_t$) out to 70% conversion. Employing the method of initial rates with data collected to 15% conversion, the order in $SiCl_4$ was revealed

SCHEME 6

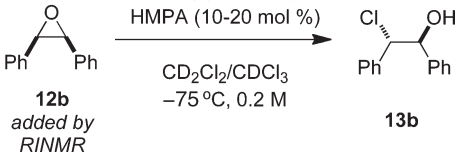

to be zero-order. Upon going from 1 to 10 equiv of $SiCl_4$, only small changes in initial rate were observed, and overall first-order behavior was maintained throughout. In order to determine the order in HMPA, changes in the first-order rate constant (k_{obs}) were examined within the range of 10−20 mol % catalyst (Figure 14D). This narrow range of catalyst concentrations was employed because of the rate of these reactions. Despite these limitations, this concentration range still contains the synthetically relevant catalyst loadings. Plotting ln[HMPA] against ln(k_{obs}) revealed that the order in HMPA was 2.2 (R^2 = 0.9769). On the basis of all these results, the following rate equation for the epoxide opening was determined: d(**2**)/dt = k_{obs}[$SiCl_4$]^0[**12b**]^1 (where k_{obs} = k[HMPA]^2).

The results of the RINMR kinetic study of the epoxide opening suggest a mechanism that is consistent with the larger picture of Lewis base catalyzed−Lewis acid activated reactions such as the silyl ketene acetal addition described in Section 7.2. Furthermore, these observations are consistent with studies by Fu on the *N*-oxide catalyzed opening of *meso* epoxides with $SiCl_4$.[25a] Foregoing studies have shown the existence of a 3:1 HMPA/$SiCl_4$ resting state (coordinatively saturated complex **i**, Scheme 7).[3a] Dissociation of one molecule of HMPA from **i** would then generate the coordinatively unsaturated, cationic silicon complex **ii**. Because the rate dependence on [HMPA] observed for the epoxide opening of **12b** is second-order, the equilibrium between **i** and **ii** must be extremely rapid compared to subsequent steps in the catalytic cycle (k_2 and $k_{-2} \gg k_3$). This conclusion is supported by the fact that the addition of silyl ketene acetal **7** is at least 20-fold faster than the epoxide opening.[29] Therefore the dissociation of HMPA, which is kinetically significant in the case of the silyl ketene acetal addition (giving rise to a 2/3 order in HMPA), is simply a pre-equilibrium step and does not factor into the rate equation in this case, leading to the simple second-order dependence on HMPA. In other words, the concentration of the coordinatively unsaturated complex **ii** is at steady state. Attack of the chloride ion of the activated complex **iii** would then occur to afford the product complex **iv**, which would release the catalyst and the silylated product **14**, allowing for catalyst turnover.

The knowledge that two phosphoramide molecules are present in the active chiral Lewis acid complex suggested that a dimeric phosphoramide, such as (*R*,*R*)-**9ac**, might provide higher selectivity. However, when this hypothesis was tested, it was found that the dimeric phosphoramide (*R*,*R*)-**9c** actually gave lower selectivity in the reaction with **12b**, suggesting that mechanistic differences between these two catalyst structures may exist (Scheme 8). So even though these studies did not lead to an improved phosphoramide catalyst for

(27) Denmark, S. E.; Barsanti, P. A.; Beutner, G. L.; Wilson, T. W. *Adv. Synth. Catal.* **2007**, *349*, 567–582.

(28) Schmid, R.; Sapunov, V. N. *Non-Formal Kinetics*; Verlag Chemie: Weinheim, 1982.

(29) Approximate half-lives for the two reactions under similar conditions support this claim: aldolization of **7**, $t_{1/2}$ = ca. 80 s (0.020 M in **7**, −60 °C); epoxide opening of **12b**, ca. 1800 s (0.025 M in **12b**, −75 °C).

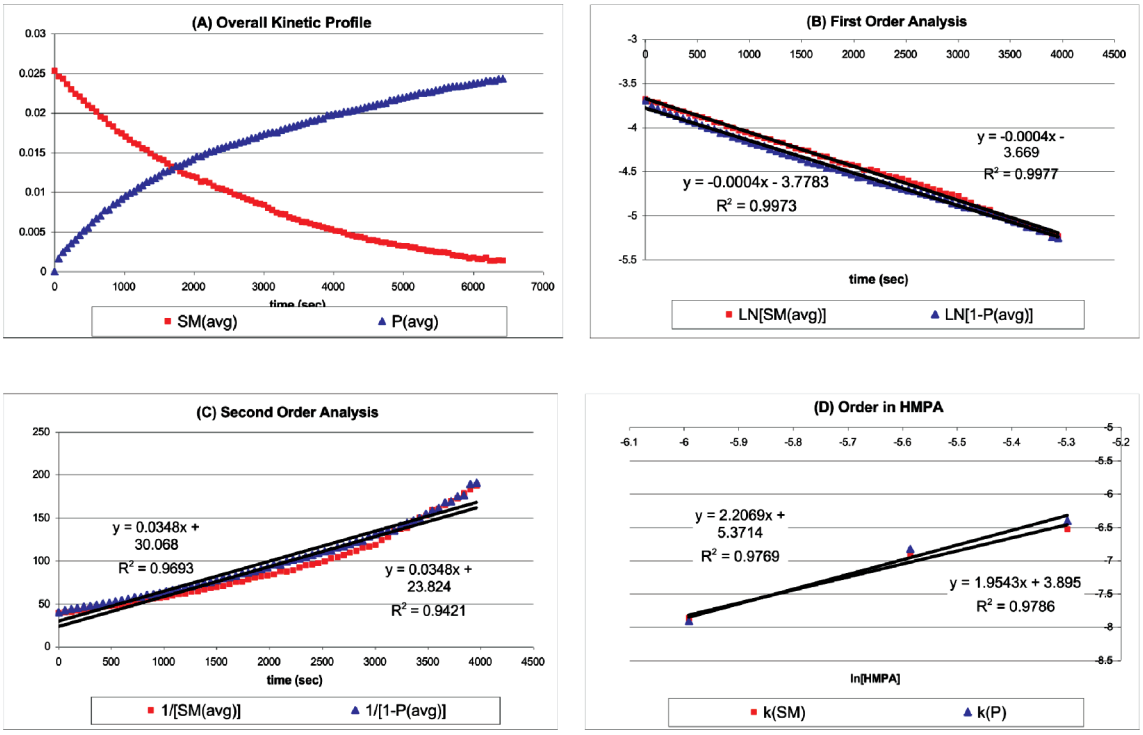

FIGURE 14. Kinetic plots for opening of **12b**: (A) overall kinetic profile, (B) first-order analysis, (C) second-order analysis, (D) order in HMPA.

SCHEME 7

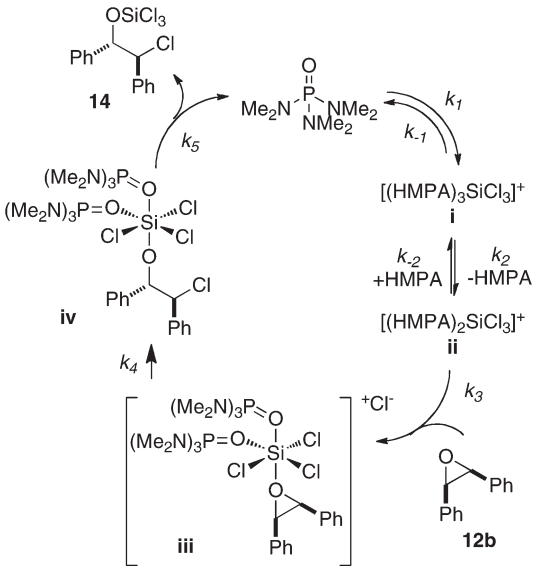

desymmetrization, these results did lead to the understanding that the complex **i** was a powerful *in situ* generated chiral Lewis acid catalyst that might have broader applications to other electrophiles. In subsequent years, these kinetic studies served as the starting point for the development of a wide array of highly selective, asymmetric Lewis base catalyzed–Lewis acid promoted processes.[30] This outcome nicely illustrates

(30) (a) Denmark, S. E.; Beutner, G. L.; Wynn, T.; Eastgate, M. D. *J. Am. Chem. Soc.* **2005**, *127*, 3774–3789. (b) Denmark, S. E.; Fan, Y. *J. Org. Chem.* **2005**, *70*, 9667–9676. (c) Denmark, S. E.; Heemstra, J. R., Jr. *J. Org. Chem.* **2007**, *72*, 5668–5688. (d) Denmark, S. E.; Wilson, T. W.; Burk, M. T.; Heemstra, J. R., Jr. *J. Am. Chem. Soc.* **2007**, *129*, 14864–14865.

SCHEME 8

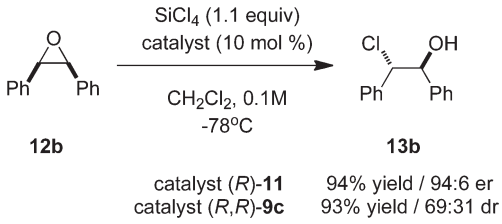

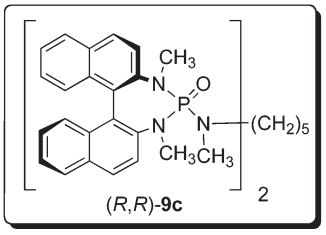

how mechanistic insights, even those that may seem beyond the scope of traditional methods, can be vital to the design of new and valuable synthetic methods.

Discussion

1. Realization of Design Goals. At the outset of this enterprise, we set ourselves ambitious goals for the capabilities of this instrument, and these goals were all realized. The universality of the injection system allows for the use of any reagent that is compatible with the glass reservoir, the ceramic piston of the metering pump, the Teflon delivery lines, and the titanium injection tube. Indeed, in addition to the reagents described in the case studies above, we have also injected highly reactive compounds such as organomagnesium and organolithium reagents as well as strong Lewis acids

such as tin tetrachloride. The modular construction of the reservoir allows for these reagents to be transferred in the laboratory under an inert atmosphere and then transported to the NMR laboratory and connected to the apparatus without compromising the integrity of the reagent by exposure to the atmosphere. Accurate calibration allowed access to different reaction temperatures that are limited only by the variable temperature controller in the NMR instrument.

The greatest challenge in the design was the ability to accurately and reproducibly deliver a known amount of a reagent for kinetic measurements. Although many iterations of the injection tip were required, in the end, the collection of reproducible kinetic data in a number of case studies provided confidence that even that goal was achieved.

2. Limitations. A number of limitations are readily apparent. First, the time delay after injection and before data accumulation represents a built in limitation for the analysis of extremely fast reactions. Currently, efficient injection and mixing can be accomplished at a minimum of 1 s. Adding a second of delay before acquisition means that a 2-s blockout window is imposed. In addition, the pulse frequency is limited by the relaxation times (T_1) of the relevant nuclei. This limitation is general for all NMR techniques and will be of importance only when quantitative measurements are desired.

Finally, whereas multiple injections of a given reagent can be made to observe, *inter alia*, catalytic turnover, reaction robustness, and influence of stoichiometry, the current design allows only two components to be mixed.

3. Design Modifications. Both up and down linear actuator speeds are set with manually adjusted valves. Arriving at the desired values can take some time as there is no way to know, without trial and error, what the speeds are. If not correct on the first try, a manual adjustment is made to the thumbscrew on the valve. Several tries may be necessary for each direction. Also, the actuators are gas-operated valves, and since gas is very compressible, linear operational speed is more a goal than a reality.

The responsiveness of the actuators could be improved with digitally controlled, hydraulically operated valves. These valves would be accompanied by the necessary electronic control to set the speeds to the desired value within a certain resolution (0.1 s). This reproducibility could be achieved with a hydraulically operated valve because fluid is not generally compressible.

A design element that is unique to this system, but not a limitation, is the significant dead volume required to deliver the reagent from the reservoir to the injector. Because the reagent is delivered at this distance via a metering pump and the injector has to be lifted vertically to insert into the magnet, the Teflon line connecting the pump to the titanium tube is rather long (5−6 ft.) and the overall dead volume of the system is ca. 6 mL. Thus it is prudent, if possible, to inject the less precious component of a reaction since only several microliters are actually used. A possible solution would be to have a volume of the expensive reagent located on the inject housing. The Ivek fluid pump could use an inexpensive fluid to drive a mechanical cylinder located in the tubing that would then drive the more expensive reagent. The two fluids could be isolated in this way. Leakage and accuracy problems would have to be overcome but are not insurmountable. This problem is also avoided with shielded magnets.

Conclusions

The design, construction, validation, and implementation of a Rapid Injection NMR apparatus have been described. The apparatus has proven reliable and robust in a number of mechanistic studies wherein currently available methods for the acquisition of accurate kinetic data were not suitable. The instrument has been designed to provide universal application for the real time analysis of fast chemical reactions. The authors urge interested parties to not embark on the construction of their own instrument and invite those whose research problems might be amenable to this kind of analysis to contact the corresponding author for access to the apparatus described herein.

Acknowledgment. The authors are grateful to the National Science Foundation for generous financial support (NSF CHE-9803124, 0105205, 0414440 and CHE 0717989).

Supporting Information Available: Detailed schematics and plans for construction of the instrument, volume and temperature calibration data and spectra, and a selection of movies (in QuickTime format) that illustrate the injection and mixing process. This material is available free of charge via the Internet at http://pubs.acs.org.